Geophys. J. Int. (1995) **120**, 87–96

S-wave anisotropy off Lofoten, Norway, indicative of fluids in the lower continental crust?

Rolf Mjelde,[1] Markvard A. Sellevoll,[1] Hideki Shimamura,[2] Takaya Iwasaki[3] and Toshihiko Kanazawa[4]

[1] *Institute of Solid Earth Physics, Allégt.* 41, *University of Bergen,* 5007 *Bergen, Norway*
[2] *Laboratory for Ocean Bottom Seismology, Hokkaido University, Sapporo* 060, *Japan*
[3] *Earthquake Research Institute, Tokyo University, Yoyoi 1-1-1, Tokyo* 113, *Japan*
[4] *Laboratory for Earthquake Chemistry, Tokyo University, 7-3-1 Hongo, Tokyo* 113, *Japan*

Accepted 1994 June 28. Received 1994 June 7; in original form 1994 February 7

SUMMARY

P- and *S*-wave velocity models along two 145 and 175 km long perpendicular profiles on the continental shelf off Lofoten, northern Norway, have been obtained from a study of nine three-component ocean-bottom seismographs. The *S*-wave model has been achieved from a study of the high-quality, horizontal component data. On one OBS the *S*-wave reflection from the Moho can be followed almost continuously from vertical to wide-angle incidence. This unique observation indicates the presence of about 10 per cent *S*-wave anisotropy in the lower crust along the NE–SW profile. No such anisotropy is observed along the NW–SE profile, and it is suggested that the inferred anisotropy might be caused by liquid-filled microcracks or pores aligned vertically along this profile. The vertical NW–SE alignment of the microcracks/pores might be a result of the present-day stress-field (the maximum compressive stress trends NW–SE), or it might be influenced by recent ductile strain fabrics or by ductile strain fabrics inherited from earlier deformation episodes. Another possible explanation for the inferred anisotropy might be alignment of anisotropic minerals. Many highly anisotropic minerals like olivine, pyroxene and hornblende can be excluded in this case, since the inferred *S*-wave anisotropy is at least three times higher than the *P*-wave anisotropy. Alignment of the mineral kyanite, however, might possibly explain the observations, since this mineral has much higher *S*-wave anisotropy than *P*-wave anisotropy. The hypothesis involving fluids is preferred since the very high seismic velocities of kyanite do not seem to be compatible with the estimated lower crustal velocity in this area ($V_p = 6.8\,\mathrm{km\,s^{-1}}$).

Key words: anisotropy, continental crust, Norway, *S* waves.

INTRODUCTION

Studies of seismic data have traditionally been, and are still, mostly concerned with *P* waves. This is related to the fact that *P* waves are easy to generate and detect, and that studying *P* waves alone has often been regarded as satisfactory for analysing geological aspects in regional geodynamic studies as well as in prospecting. It has, however, been understood that numerous geological problems can be elucidated in more detail by an integrated use of *S* and *P* waves. An illustrative example would be the additional constraints that can be placed on possible lithologies if the *S*-wave velocity is known in addition to the *P*-wave velocity (Neidell 1985).

An interesting aspect of *S* waves is their sensitivity to the orientation of cracks and microcracks indicated through numerous observations of *S*-wave splitting (Crampin 1990), and their possible sensitivity to preferred orientations of minerals and grains. Such aspects, together with the improvements of seismic sources, three-component receivers, and processing, interpretation and modelling techniques, have strengthened the view that *S* waves in many cases both can and should be studied in detail and combined with *P* waves. An extensive crustal experiment incorporating the study of *S* waves was performed in 1988 off Lofoten, northern Norway (Mjelde *et al.* 1992). In that survey, 24 three-component ocean-bottom seismographs (OBSs) covering the area from the continental shelf to the oceanic crust were used (Fig. 1).

A 2-D *P*- and *S*-wave velocity model along a profile shot on the continental shelf (profile 6; Fig. 1) was presented by Mjelde (1992). In that study an important angle-of-incidence

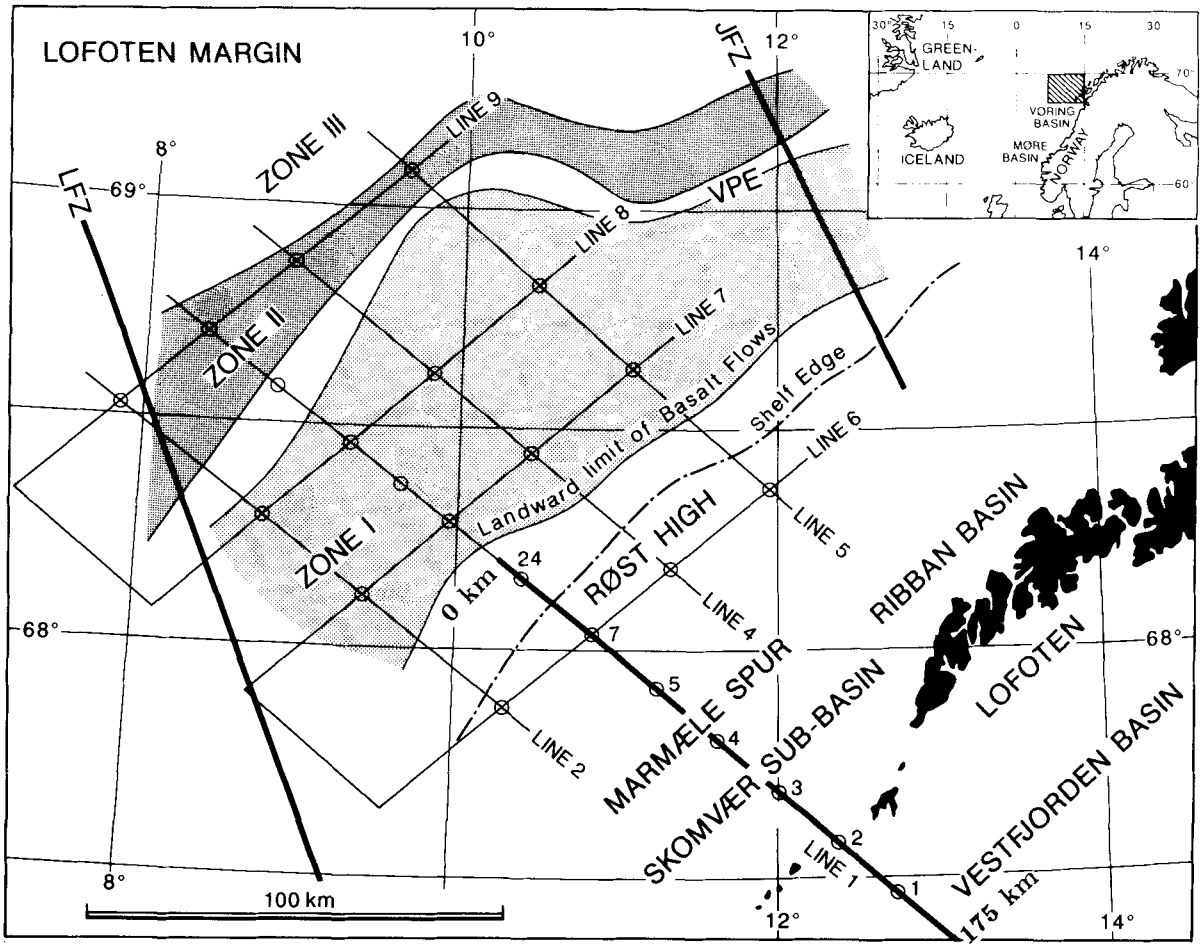

Figure 1. Main structural elements off Lofoten with position of OBSs and seismic reflection profiles shot during the 1988 survey indicated. The position of the reflection profile shot by GECO in 1987 (line 1) and described in this paper is indicated as a heavy line. VPE = the northward continuation of the Vøring escarpment, LFZ = Lofoten lineament, JFZ = Jennegga lineament, ZONE I = early Eocene flood-basalt, ZONE II = seaward-dipping reflectors, ZONE III = oceanic crust. The position of the Vøring and Møre basins are indicated in the upper right corner. Modified from Sellevoll (1988).

dependent *S*-wave anisotropy in the lower crust was discovered. This anisotropy was inferred to be consistent with some horizontal or subhorizontal layering in the lower crust. The present paper describes the 2-D *P*- and *S*-wave velocity model for the lower crust along profile 1 in Fig. 1. The data from this profile are of the same high quality as those of the previously studied profile, and the analysis of profile 1 could hopefully contribute to verify and constrain the conclusions drawn in Mjelde (1992). In addition, the two profiles are perpendicular, which should enable possible azimuthal anisotropy to be detected.

GEOLOGICAL FRAMEWORK

The study region (Fig. 1) was characterized by a compressional regime in the late Silurian to early Devonian, resulting in suturing of the Laurentia (Greenland) and the Baltica (Scandinavia) plates and the formation of the Caledonides (Bukovics *et al.* 1984; Bøen, Eggen & Vollset 1984; Gage & Dore 1986; Soper *et al.* 1992). The crystalline basement in Lofoten is believed to represent an exhumed deep section of the crust (Chroston & Brooks 1989). Within the Lofoten archipelago, Archaean and Proterozoic rocks lie within a belt of basement gneisses to the west of the Caledonian nappes. The Lofoten suite comprises high-grade metamorphic rocks of granulite and amphibolite facies.

No boreholes have been drilled on the Lofoten margin, and the present model of this margin (Mokhtari 1991) has been based primarily on the gross stratigraphic relationships observed along the shelf. The margin has been dominated in post-Caledonian time by extensional tectonics, and pre-Cretaceous sequences, with a maximum thickness of about 5 km in the Vestfjorden Basin, are present along most of the shelf (Mjelde *et al.* 1993).

The late Jurassic–early Cretaceous extension led to major faulting activity along the entire margin, partly as reactivation of older fault zones, generally creating slightly rotated fault blocks and causing subsequent subsidence along major rift systems (Rønnevik, Eggen & Vollset 1983; Bøen *et al.* 1984; Hinz, Dostman & Hansch 1984; Mutter 1984; Skogseid & Eldholm 1989; Mokhtari 1991). Sedimentary sequences of Cretaceous age locally exceeding 5 km in thickness are preserved on the Lofoten shelf within the Ribban Basin (Fig. 1). The early Cenozoic extension axis shifted westward with respect to the Jurassic–Cretaceous episode, with continental separation in the earliest Eocene.

Tertiary sediments are very thin or absent over the Lofoten shelf. It is uncertain whether Palaeogene sediments are eroded by post-depositional uplift or whether the shelf remained emergent throughout this period. The Lofoten shelf appears to have been a sediment bypass area in Neogene time.

DATA ACQUISITION AND PROCESSING

The OBS data were acquired during the summer of 1988 using R/V *Håkon Mosby,* University of Bergen. The scientific programme comprised simultaneous seismic reflection, seismic refraction and gravimetric measurements. The positions of the seismic reflection/refraction profiles and ocean-bottom seismographs (OBSs) are indicated in Fig. 1. The effective length of the streamer used was 1950 m. Seismic reflection data were not acquired along profile 1 during this experiment, since this profile coincides with a high-resolution seismic reflection line acquired by the Norwegian Petroleum Directorat in 1987.

Four Bolt 1500 C airguns with a total volume of 79 l (4800 in^3) were used as the source. The source was operated at a depth of 21 m and the shotpoint inverval was 240 m (2 min).

The OBS instruments used were developed and built by the geophysical institutes at Hokkaido and Tokyo Universities (Shimamura 1988). The analogue OBS instruments have three orthogonal components (4.5 Hz, gimbal-mounted geophones), one vertical and two horizontal. The instruments can record continuously for 14 days within the frequency range of 1 to 30 Hz (−3 dB).

Twenty-four OBS instruments were used to acquire the seismic refraction data, of which seven were located at 20–25 km intervals along profile 1 and four along profile 6 (Fig. 1). Unfortunately, the magnetic tapes from OBS 2 were blank; the acquisition thus provided wide-angle data from six OBS instruments located along profile 1. The analysis of the data from the remaining profiles is presented in Mjelde *et al.* (1992).

Velocity filtering and several deconvolution schemes have been applied to the OBS data (digitized at Hokkaido and Tokyo Universities) to help identification of the different *S* phases, as described in Mjelde (1992). However, the quality of the raw data is excellent, and the data examples presented in this paper have been bandpass filtered (6–13 Hz) only. The data are plotted with Automatic Gain Control (4 s window), and the interpretation of the data was carried out on displays with traveltime reduced by 8 km s^{-1}.

RESULTS AND DISCUSSION

Modelling procedure

Figure 2 shows the seismogram from the vertical component of OBS 7 profile 1 (from Mjelde *et al.* 1993). The *P* waves from the vertical components have been modelled by use of 2-D kinematic (traveltime) ray tracing. The resulting *P*-wave model shown in Fig. 3 has been obtained by the combined use of multichannel seismic reflection data (Fig. 4) and the OBS data (Mjelde *et al.* 1993). The uncertainty in the Moho depth and velocities (both *P* and *S*) is estimated to be ±1 km and ±0.1 km s^{-1} respectively (Mjelde 1992; Mjelde *et al.* 1992). Figs 5–7 show the seismograms from one of the two horizontal components of OBS 7 (profile 1 and 6) and OBS 5 (profile 1). The *P*-wave model (Fig. 3) has been used as a basis for 2-D kinematic ray-tracing modelling of the *S* waves interpreted from the horizontal components. This procedure is based on the assumption that the structural interfaces (iso-velocity lines) are the same for *P* and *S* waves. Calculated traveltimes indicated in the seismograms represent critical refractions (head waves), unless otherwise specified. Only one of the horizontal components is presented for each site since the waveforms recorded at each of the two (non-orientated) horizontal components were

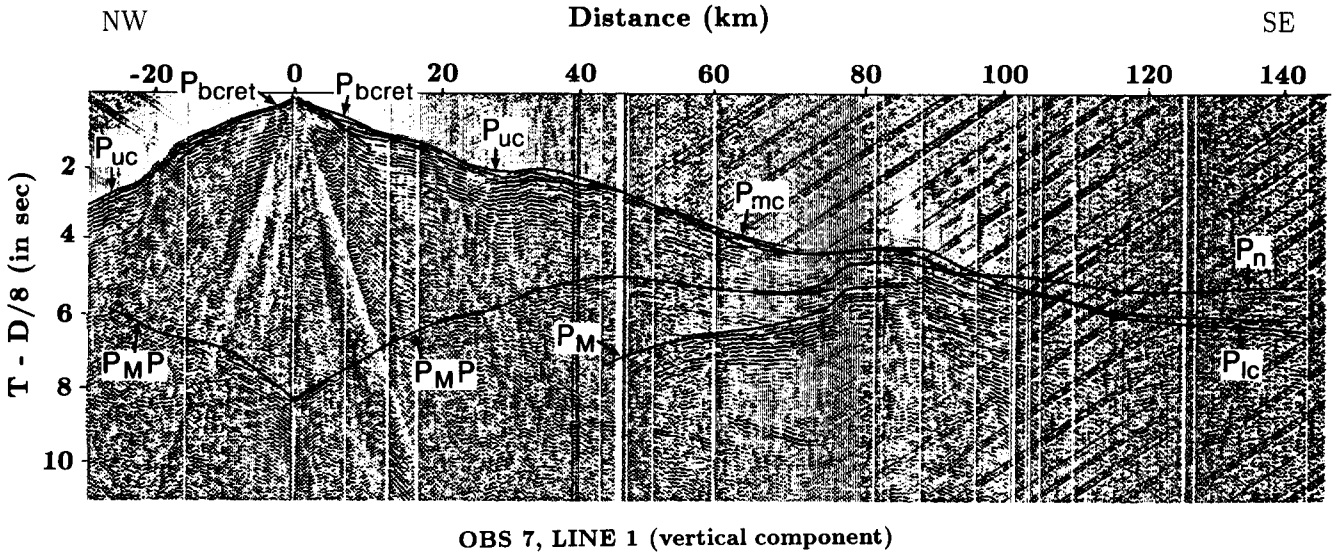

Figure 2. OBS 7 vertical component shot along profile 1 with *P*-wave traveltime curves (solid lines) calculated from the model in Fig. 9 indicated (from 2-D raytracing). P_{bcret} = base Cretaceous refraction, P_{uc} = upper crust refraction, P_{mc} = middle crust refraction, P_{lc} = lower crust refraction, P_n = Moho refraction, P_MP = Moho reflection, P_M = upper mantle reflection. The raw data of this vertical component are presented in Mjelde *et al.* (1993).

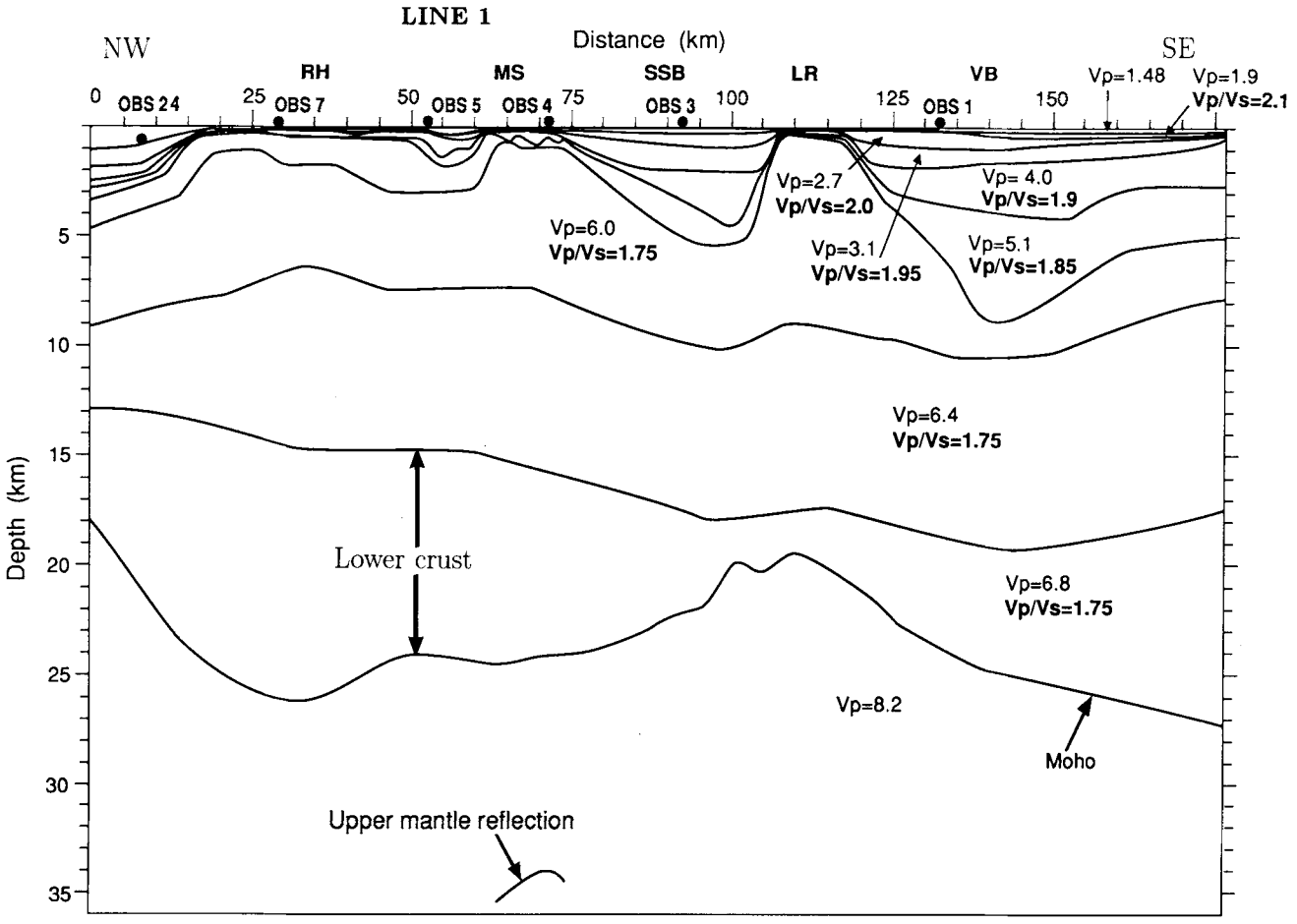

Figure 3. Model of *P*-wave velocity (V_p in km s^{-1}) and V_p/V_s ratio for profile 1. RH = Røst High, MS = Marmæle Spur, SSB = Skomvær sub-Basin, LR = Lofoten Ridge, VB = Vestfjorden Basin.

very similar. This indicates that the horizontal geophones were probably rotated at 30°–45° from the azimuth of the shot profiles. The relatively low amplitude of the *S*-wave arrivals on the vertical components seismograms reaffirms the identification of these phases (compare Figs 2 and 5). The important S_MS phase, for instance, is observed clearly only on the horizontal components. As for the modelling of profile 6 (Mjelde 1992), it has been assumed that the *P* waves are converted to *S* waves at the sea-floor, which represents a very high impedance contrast (the thickness of the Tertiary sediments is negligible along the profile).

We emphasize that the V_p and V_p/V_s model in Fig. 3 is a result of traveltime modelling only. Dynamic modelling with calculation of velocity gradients has not been included, due to uncertainties in the recorded amplitudes, making such modelling unreliable for this data set (Mjelde *et al.* 1993). The same applies to the study of particle diagrams with regard to *S*-wave splitting. The amplitude problem further prohibits the horizontal components to be orientated into an in-line and a cross-line component.

The *P*-wave model and upper crustal *S*-wave model

The crustal structure along the profile is characterized by a succession of basement highs and deep basins (Fig. 3). Sequences of Tertiary sediments are very thin or partially absent along the profile. Three Cretaceous sequences are identified with *P*-wave velocities of 2.7 km s^{-1} ($V_p/V_s = 2.0$), 3.1 km s^{-1} ($V_p/V_s = 1.95$) and 4.0 km s^{-1} ($V_p/V_s = 1.9$) respectively. The 5.1 km s^{-1} refractor coincides with the base Cretaceous reflector interpreted and mapped in detail on the shelf by Mokhtari, Pegrum & Sellevoll (1989). The thickness of the pre-Cretaceous sediments ($V_p/V_s = 1.85$) varies considerably along the profile, with a maximum thickness of about 5 km in the Vestfjorden Basin.

The 6.0 km s^{-1} refractor is interpreted to represent the top of crystalline basement. The crystalline crust is divided into three layers; an upper, an intermediate and a lower crustal layer with *P*-wave velocities of 6.0 km s^{-1} ($V_p/V_s = 1.75$), 6.4 km s^{-1} ($V_p/V_s = 1.75$) and 6.8 km s^{-1} respectively. The interfaces between these layers can be interpreted as first-order discontinuities on at least one OBS (Mjelde *et al.* 1993). The velocities found correspond in general with earlier studies (Sellevoll 1973; Sellevoll & Thanvarachorn 1977; Drivenes *et al.* 1984). The V_p/V_s model for the sediments and upper crystalline crust is presented in detail by Mjelde & Sellevoll (1993).

In addition to these discontinuities, which explain the arrivals observable along the entire profile, some local upper crustal wide-angle reflections are observed in the Skomvær sub-Basin (Figs 5 and 7). These reflections, which indicate local upper crustal heterogeneities in this area, are not

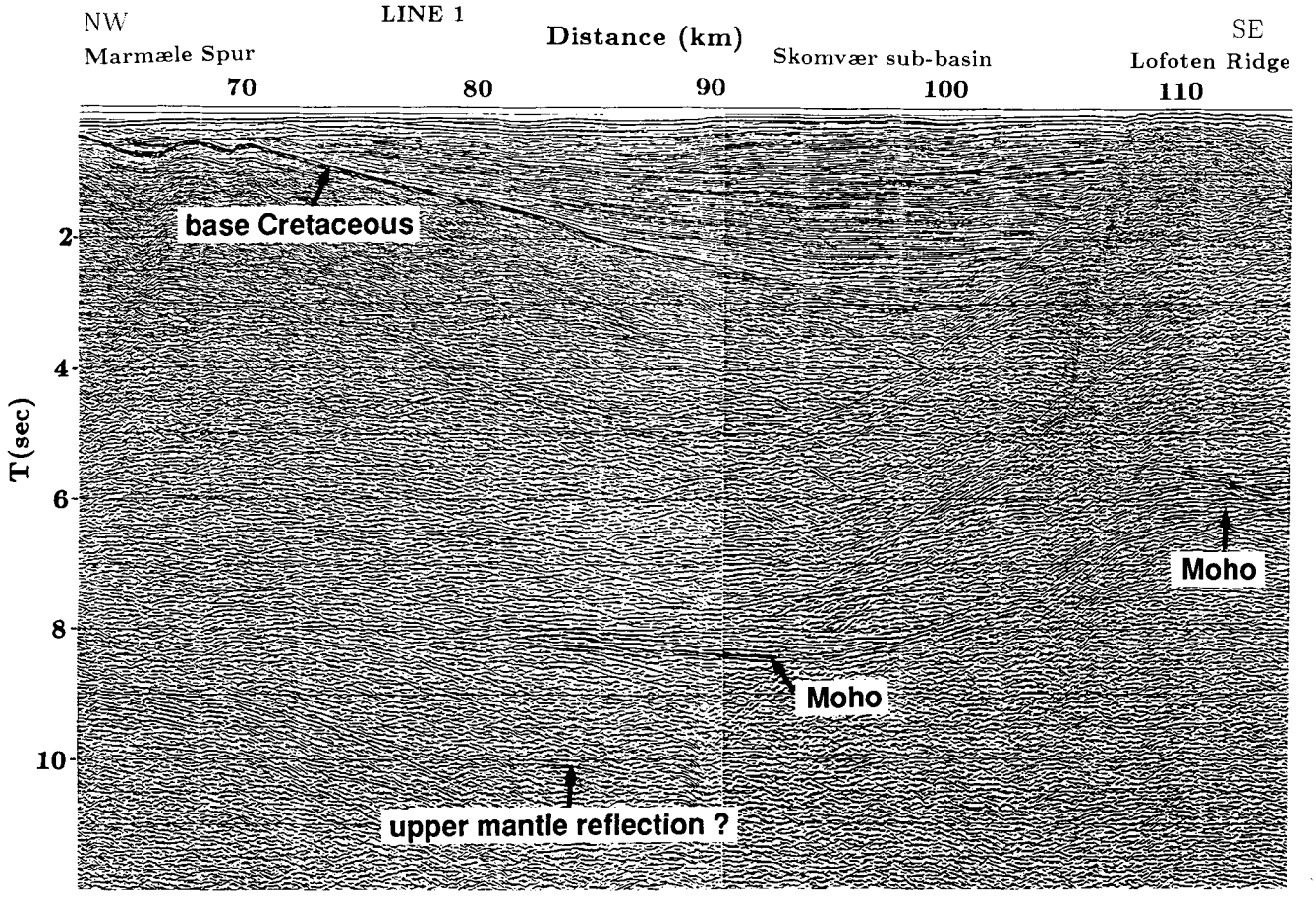

Figure 4. Part of the unmigrated multichannel reflection profile shot in 1987 by GECO. See Fig. 1 for location (line 1, from NE to SW). From Mjelde *et al.* (1993).

included in the model (Fig. 3) since they do not seem to have an important influence on the first-order velocity distribution.

The lower crust varies considerably in thickness, from about 11.5 km under the Røst High to about 2 km under the Lofoten Ridge. The lower crust thus seems to have had rheological properties that were markedly different from that of the shallower crust during the earlier extension episodes (Mjelde *et al.* 1993); the lateral variations of the thickness of the lower crust indicate that there has been significant lateral ductile flow of material in this portion of the crust.

The V_p/V_s model in the lower crust

During the study of profile 6 it was discovered that the S-wave reflections from Moho (S_MS) deviated strongly from that predicted from an isotropic model (Mjelde 1992; Fig. 6). The modelling of the S_MS phases showed that a V_p/V_s ratio of 1.95 ($V_s = 3.5\,\mathrm{km\,s^{-1}}$) in the lower crust satisfied the observations for waves propagating vertically. For larger offsets (wide angles), however, the isotropic model predicted significantly later arrival times than observed.

Mjelde (1992) argued that the only simple explanation for the S_MS deviation seen on profile 6 is seismic anisotropy: the S-wave velocity seems to increase with increasing angle of incidence. It was further argued that the anisotropy (which was not observed for the P_MP phase) was probably restricted to the lower crust based on the modelling of an arrival from the top of the middle crust ($P_MP_{lc}S$ on Fig. 6), and it was inferred that an S wave propagating in the lower crust with an angle deviating about 60°–70° from the vertical apparently had an approximately 14 per cent higher velocity than a vertically propagating wave. The strong mode conversions at the sea-floor for vertically propagating waves can probably be ascribed to tilted sedimentary layers (Mjelde *et al.* 1992), and the model conversions at the Moho might indicate dipping upper mantle structures, upper mantle anisotropy or rough Moho topography (on a small scale).

To explain the lower crustal anisotropy on line 6, a model consisting of horizontally aligned penny-shaped liquid-filled microcracks with a crack density (CD) of 0.1 ($\mathrm{CD} = N a^3/v$ where N is the number of cracks of radius a and half-thickness d in volume v) and an aspect ratio (AR) of 0.05 ($\mathrm{AR} = d/a$) was suggested. According to this model, the observed (apparent) S-wave anisotropy of about 14 per cent might correspond to a real S-wave anisotropy in the order of 10 per cent (and a real P-wave anisotropy of about 3 per cent which is too small to be detected; see Fig. 8).

If the model with horizontal or subhorizontal microcracks in the lower crust were correct, one would also expect to observe the strong deviation with offset of the S_MS arrival along profile 1. Fig. 5 demonstrates that this is not the case; the S_MS arrival can be modelled using a constant (isotropic)

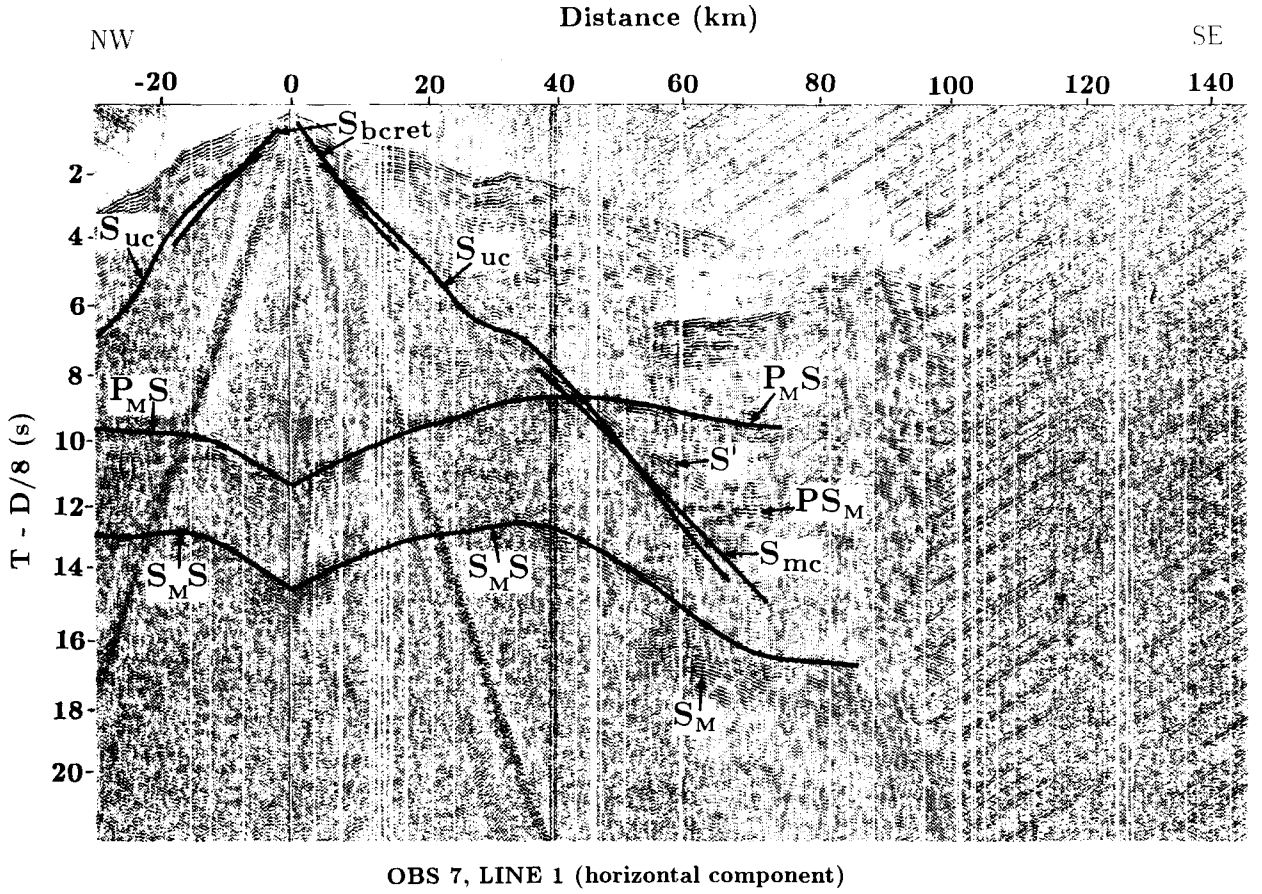

Figure 5. OBS 7 horizontal component shot along profile 1 with *S*-wave traveltime curves from the model in Fig. 9 indicated (calculated from 2-D ray tracing). S_{bcret} = base Cretaceous refraction, S_{uc} = upper crust refraction, S_{mc} = middle crust refraction, S_MS = Moho reflection, P_MS = mode conversion at the Moho, S' = local upper crustal heterogeneities, S_M = upper mantle reflection, PS_M = upper mantle mode conversion. The raw data of this horizontal component are presented in Mjelde & Sellevoll (1993).

V_p/V_s ratio of 1.75 ($V_s = 3.9\,km\,s^{-1}$) in the lower crust. A model that satisfies the observations along both profies is shown in Fig. 8; this is the same model as described above, but with the liquid-filled microcracks aligned vertically along profile 1. The left-hand panel of the figure demonstrates how the velocity of the quasi-*SV* wave increases from vertical incidence (*Z*) to 45° angle-of-incidence in the NE direction (parallel to profile 6, perpendicular to the strike of the cracks), and the right-hand panel demonstrates that the velocity of the quasi-*SV* wave is constant (and high) for all angles-of-incidence in the NW direction (parallel both to profile 1 and the strike of the cracks). This anisotropic model explains the traveltime observations for both studied profiles. Lateral velocity variations can be ruled out as an alternative explanation, since a direct estimate of the velocity anisotropy can be obtained below OBS 7, due to the detection of near-vertically propagating waves acquired along both profiles here.

Heat-flow measurements give very low values of around 1 HFU in the region (Grønlie, Heier & Swanberg 1977), and we estimate the temperature in the lower crust (15–25 km depth) to be about 225–375 °C in this area. The low temperature in the lower crust might imply that the lower crustal rocks are semi-brittle, and not ductile which is often assumed for rocks at lower crustal depths (the temperature for brittle–ductile transition is about 450 °C for malfic rocks; Rutter & Brodie 1992). This might explain the presence of the inferred microcracks, since open microcracks aligned vertically probably cannot remain stable for a significant amount of time in a ductile lower crust. The apparent absence of microcracks below 2–5 km depth in the brittle upper and middle crust can be explained by the pore pressure in this part of the crust being generally less than lithostatic (Hyndman & Shearer 1989). There will thus be a high effective pressure closing the cracks at these relatively shallow depths. The opening of microcracks in the lower crust is enhanced by the higher temperatures at these depths which cause the effective pressure to decrease to near zero, allowing thin pores to stay open (Hyndman & Shearer 1989).

The microcracks are, according to the model described above, inferred to be aligned vertically along profile 1. Fig. 9 shows that this profile coincides with the direction of the present-day maximum compressive stress in the area. It is thus possible that the inferred microcracks are aligned vertically in the NW–SE direction as a result of the present-day stress-field (consistent with the possible shallow anisotropy described by Mjelde & Sellevoll 1993).

Alternatively, it must be considered as a possibility that presence of fluids in the lower crust might enhance ductile deformation even at moderate temperatures, thus inhibiting the formation of vertically aligned open microcracks at these

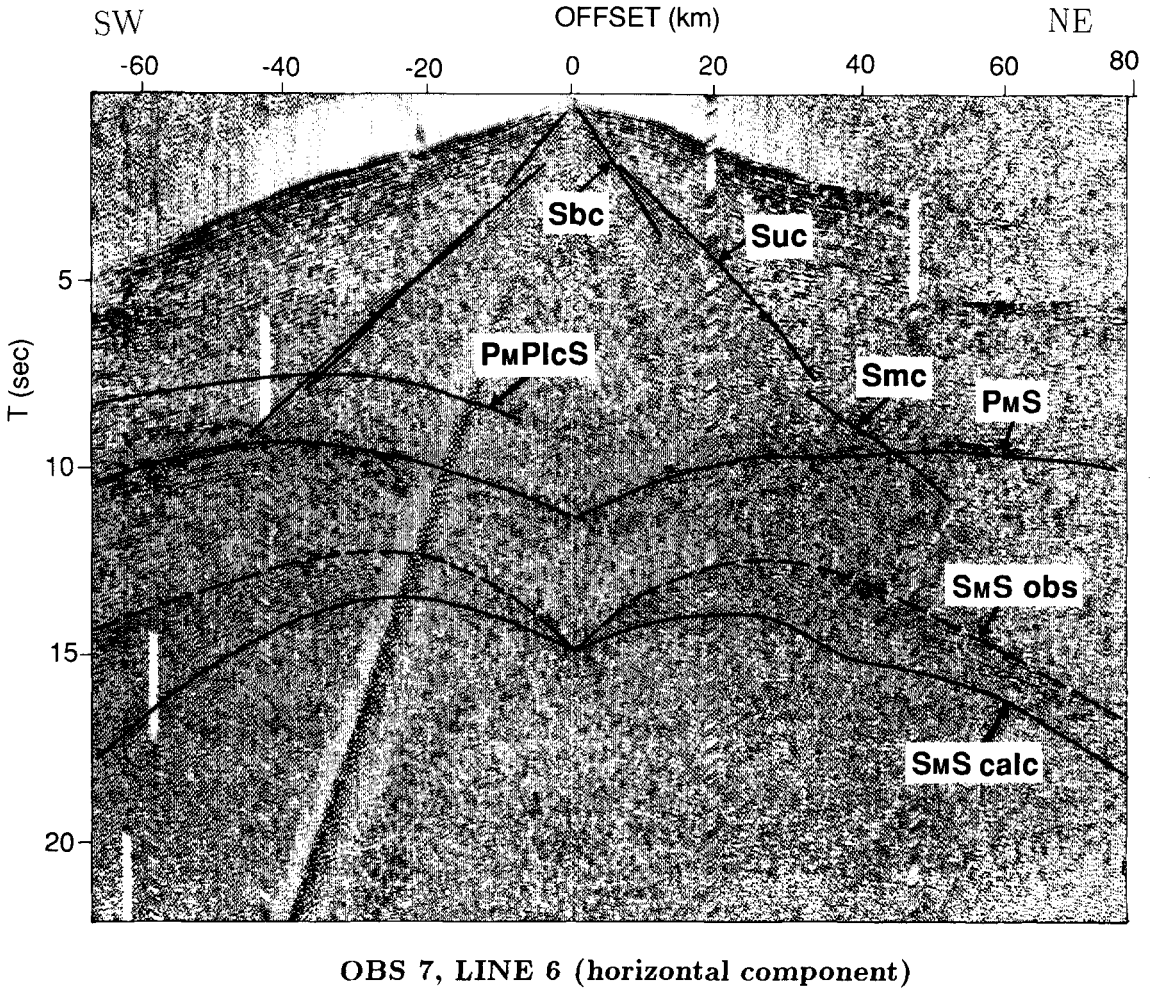

Figure 6. OBS 7 horizontal component shot along profile 6 with *S*-wave traveltime curves calculated from 2-D ray tracing indicated (reduced velocity 8.0 km s^{-1} 6–13 Hz bandpass filtered). S_{bc} = base Cretaceous refraction, S_{uc} = upper crust refraction, S_{mc} = middle crust refraction, $P_M P_{lc} S$ = mode conversion at the top of the lower crust, $S_M S$ = Moho reflection, $P_M S$ = mode conversion at the Moho. Dashed and solid lines represent observed and calculated traveltime curves respectively. From Mjelde (1992).

depths. Profile 1 is coincident with the inferred direction of maximum crustal ductile flow active during the Jurassic–Cretaceous and older extension episodes (Mjelde *et al.* 1993). The alignment of pore space might thus be influenced by ductile strain fabrics inherited from these earlier deformation episodes, or by present ductile strain fabrics in case of a still active ductile deformation (enhanced by the presence of fluids). According to this model the lower crustal alignment of fluid-filled pore space might be independent of the present-day stress-field in the area.

Alignment of fluid-filled pore space might not, however, be the only possible explanation to the inferred anisotropy. Laboratory measurements on lower crustal rocks exposed at the surface have shown that these rocks are, in many cases, highly anisotropic due to alignment of minerals (Babuska & Cara 1991). Many highly anisotropic minerals can in our case be excluded, however, since the estimated *S*-wave anisotropy is at least three times higher than the *P*-wave anisotropy. Important minerals that have similar *P*- and *S*-wave anisotropies include olivine, and chain silicates like pyroxenes and hornblende. Anisotropy due to fine-scaled layering can be excluded for the same reason.

The mineral kyanite, however, has an *S*-wave anisotropy about five times higher than the *P*-wave anisotropy (Belikov, Aleksandrov & Ryzhova 1970). Kyanite can be stable at lower crustal depths in this area (Richardson, Gilbert & Bell 1969), and significant amounts of kyanite have been found in shear zones within eclogite facies (deep crustal) rocks in the Bergen Arcs, southern Norway (Fountain *et al.* 1994). These kyanite-bearing shear zones have much higher *P*-wave velocities (8.5–9 km s^{-1}) than the estimated lower crustal *P*-wave velocity in our study area (6.8 km s^{-1}). The 6.8 km s^{-1} velocity represents a mean lower crustal velocity, however, and it could be argued that the lower crust might possibly consist of high-velocity kyanite-bearing shear zones within a significantly lower-velocity 'matrix'. In order to explain the inferred azimuthal *S*-wave anisotropy, the kyanite mineral must have some azimuthal orientation, either in steeply aligned zones between interfingering lenses, or along more horizontally layered zones with strong azimuthal orientation of the kyanite.

Magnetotelluric measurements showing high electrical conductivity in the lower crust have often been taken as

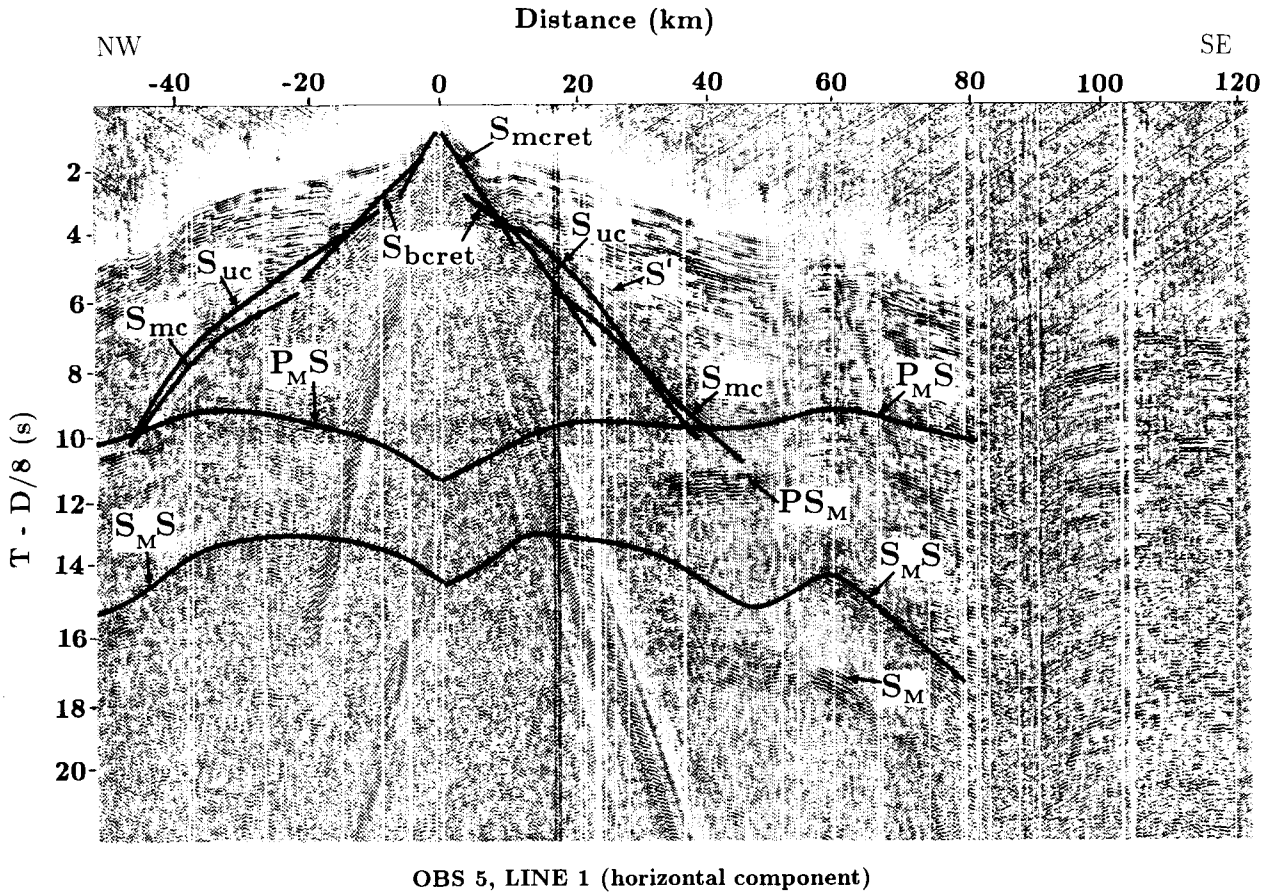

Figure 7. OBS 5 horizontal component shot along profile 1 with *S*-wave traveltime curves from the model in Fig. 9 indicated (calculated from 2-D ray tracing). S_{mcret} = middle Cretaceous refraction, S_{bcret} = base Cretaceous refraction, S_{uc} = upper crust refraction, S_{mc} = middle crust refraction, S_MS = Moho reflection, P_MS = mode conversion at the Moho. S' = local upper crustal heterogeneities, S_M = upper mantle reflection, PS_M = upper mantle mode conversion. The raw data of this horizontal component are presented in Mjelde & Sellevoll (1993).

support for the hypothesis involving fluids at these depths (Hyndman & Klemperer 1989). Conductivity measurements could potentially be used to investigate whether the model with vertically aligned fluid-filled pores has more general relevance, since a strong anisotropy in the electrical conductivity would be expected if such features are present, and the pore fluid is conductive. Electrically anisotropic lower crust has been reported from the Baltic shield (Rasmussen 1988), the Canadian shield (Kurtz *et al.* 1988; Kellett, Mareschal & Kurtz 1992), and from a Precambrian terrain in Australia (Cull 1985). Preferential fluid-filled crack orientation has been suggested as one possible explanation for the inferred lower crustal anisotropy beneath these three different Precambrian shield regions (Jones 1992). The high lower-crustal conductivity can also be explained by the presence of graphite, however, and laboratory measurements of *S*-wave anisotropy in this mineral will be needed before one can evaluate whether observations of lower crustal *S*-wave anisotropy might be used to distinguish between the presence of fluids or graphite in areas with high lower-crustal conductivity. Future experiments combining vertical incidence and wide-angle seismic data with magnetotelluric measurements along several azimuths, might help to solve the much debated questions concerning the presence of fluids in the lower crust.

CONCLUSIONS

A consistent *S*-wave velocity model along two perpendicular profiles (145 and 175 km) on the continental shelf off Lofoten, northern Norway, has been obtained by studying the horizontal components of nine OBSs. The data reveal strong crustal *S* waves and *P*- and *S*-wave reflections as well as *P*-to-*S* conversions at the Moho.

On one OBS the *S*-wave reflection from the Moho can be followed continuously from vertical to wide-angle incidence. This unique observation enables the detection of about 10 per cent *S*-wave anisotropy in the lower crust along the NE–SW profile. No such anisotropy is observed along the NW–SE profile, and it is suggested as one possibility that the inferred anisotropy is caused by liquid-filled microcracks aligned vertically along this profile. The inferred vertical NW–SE alignment of the microcracks might, in this case, be a result of the present-day stress-field (the maximum compressive stress trends NW–SE).

The low temperature in the lower crust in this area might imply that the lower crustal rocks are semi-brittle, and not ductile which is often assumed for rocks at these depths. This would explain the inferred presence of the microcracks, since open microcracks aligned vertically probably cannot remain stable for a significant amount of time in a ductile lower crust.

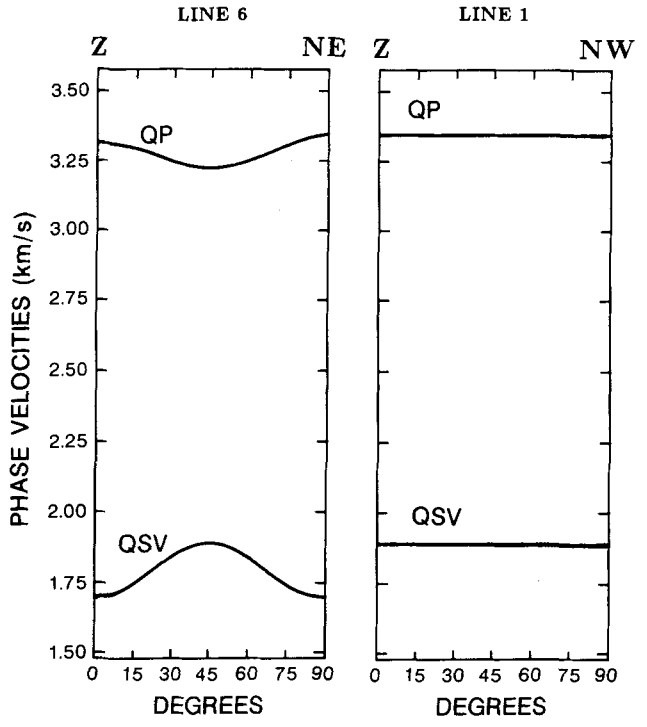

Figure 8. Variation of theoretical phase velocities with direction of propagation (degrees in angle-of-incidence) for quasi-*P* waves and quasi-*SV* waves propagating through parallel liquid-filled microcracks aligned vertically (*Z*) and striking NW–SE (along profile 1). (Penny-shaped cracks with crack density 0.1 and aspect ratio 0.05.) The left-hand panel is equivalent to wave propagation along profile 6, and the right-hand panel to propagation along profile 1. Modified from Crampin (1978) and Mjelde (1992).

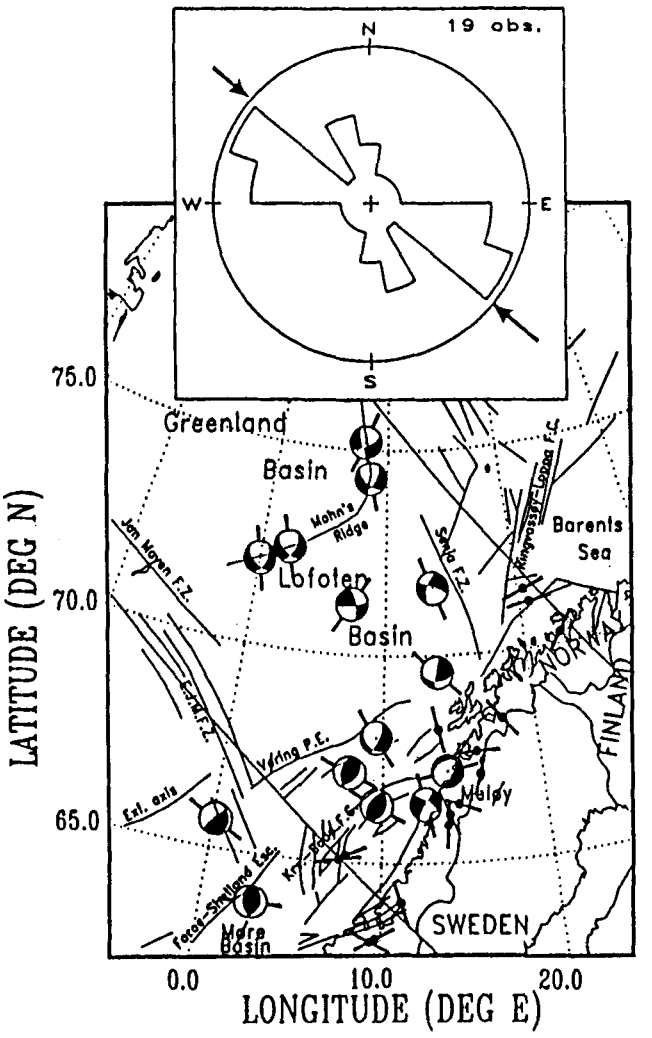

Figure 9. Focal mechanism solutions and *in situ* stress measurements (solid circles) in the region. The lines (bars) through the focal sphere projections indicate the directions of the *P* axes (maximum compressive stress). The two parallel NW–SE trending lines across the map are 'ridge push' directions. The rose diagram shows the maximum compressive stress directions from earthquakes in northern Norway and the Svalbard areas. Arrows indicate the approximate 'ridge push' direction. Notice that the direction of maximum compressive stress is very close to the strike of profile 1. From Bungum *et al.* (1990).

Alternatively, it must be considered as one possibility that the presence of fluids in the lower crust might enhance ductile deformation even at moderate temperatures, thus inhibiting the formation of vertically aligned open microcracks at these depths. In this case the alignment of pores might be influenced by ductile strain fabrics inherited from earlier deformation episodes, or by recent ductile strain fabrics.

Another possibility to explain the inferred anisotropy is to invoke a model with alignment of anisotropic minerals. Many highly anisotropic minerals like olivine, pyroxene and hornblende can be excluded, since the inferred *S*-wave anisotropy in our case is at least three times higher than the *P*-wave anisotropy. Kyanite, which has been observed in large amounts in some shear zones exhumed from lower crustal depths, has an *S*-wave anisotropy about five times higher than the *P*-wave anisotropy. This mineral might thus be considered as a possible candidate to explain the observations, although we find the fluid hypothesis more likely. This is due to the fact that the very high seismic velocities of kyanite seem to be incompatible with the estimated lower crustal velocity ($V_p = 6.8\ \mathrm{km\ s^{-1}}$).

In this paper it is demonstrated that, by use of a very simple acquisition and modelling strategy, at present we are capable of detecting a significant *S*-wave anisotropy in the lower crust, and thereby suggest important constraints on some fundamental properties of the lower crust. However, different models can explain the inferred anisotropy. In order to be able to demonstrate with certainty the presence of anisotropy and to distinguish between the different hypotheses outlined above, future acquisitions of this kind must include three-component receivers deployed along at least three different azimuths, and some sort of fan or circle-shooting should be performed. In addition, more laboratory measurements of *S*-wave anisotropy in rock-forming minerals are needed, including minerals that are generally present in very small quantities in lower crustal rocks.

ACKNOWLEDGMENTS

The authors thank Professor R. Kanestrøm (Norsk Hydro and Inst. of Solid Earth Physics (IFJ), University of Bergen

(UiB)), Dr C. Hurich (IFJ, UiB), Professor A. G. Milnes (Geological Inst. A, UiB), Dr H. Austrheim (Min. Geol. Mus., Univ. of Oslo) and Professor W. L. Griffin (CSIRO, Australia) for fruitful discussions and comments on the manuscript.

We also thank Statoil for financial support and help; in particular we would like to thank E. W. Berg, V. B. Larsen, L. B. Pedersen and K. J. Skaar.

REFERENCES

Babuska, V. & Cara, M., 1991. *Seismic Anisotropy in the Earth,* Kluwer Academic Publishers, Dordrecht.

Belikov, B. P., Aleksandrov, K. S. & Ryzhova, T. V., 1970. *Elastic Properties of Rock-Forming Minerals and Rocks,* Nauka, Moscow (in Russian).

Bøen, F., Eggen, S. & Vollset, J., 1984. Structures and basins of the margin from 62–69°N and their development, in: *Petroleum Geology of the North European Margin,* pp. 3–28, eds Spencer, A. M. *et al.* London, Graham and Trotman.

Bukovics, C., Shaw, N. D., Cartier, E. G. & Ziegler, P. A., 1984. Structure and development of the Mid-Norway continental margin, in *Petroleum Geology of the North European Margin,* pp. 407–423, eds Spencer, A. M. *et al.*, Graham and Trotman, London.

Bungum, H., Alsaker, A., Kvamme, L. B. & Hansen, R. A., 1990. Seismicity and seismotectonics of Norway and nearby continental shelf areas, *J. geophys. Res.*, **96** (B2), 2249–2265.

Crampin S., 1978. Seismic wave propagation through a cracked solid: polarization as a possible dilatancy diagnostic, *Geophys. J. R. astr. Soc.,* **53,** 467–496.

Crampin S., 1990. The scattering of *S* waves in the crust, *PAGEOPH,* **132,** 67–91.

Chroston, P. N. & Brooks, S. G., 1989. Lower crustal seismic velocities from Lofoten-Vesterålen, North Norway, *Tectonophysics,* **157,** 251–269.

Cull, J. P., 1985. Magnetotelluric soundings over a Precambrian contact in Australia, *Geophys. J. R. astr. Soc.,* **80,** 661–675.

Drivenes, G., Sellevoll, M. A., Renard, V., Avedik, F. & Pajchel, J., 1984. The continental margin/crustal structure off the Lofoten Islands, Northern Norway, in *Petroleum Geology of the North European Margin,* pp. 211–216, eds Spencer, A. M. *et al.*, Graham and Trotman, London.

Fountain, D. M., Boundy, T. M., Austrheim, H. & Rey, P., 1994. Eclogite facies shear zones—deep crustal relectors? *Tectonophysics,* **232,** 411–424.

Gage, M. S. & Dore, A. G., 1986. A regional geological perspective of the Norwegian offshore exploration provinces, in *Habitat of Hydrocarbons on the Norwegian Continental Shelf,* pp. 21–38, Norwegian Petroleum Society, Graham and Trotman, London.

Grønlie, G., Heier, K. S. & Swanberg, C. A., 1977. Terrestrial heat flow determinations from Norway, *Norg. Geol. Tidsskrift,* **55,** 153–162.

Hinz, K., Dostman, H. J. & Hansch, J., 1984. Structural elements of the Norwegian Sea continental margin, *Geol. Jahrb.,* **A75,** 193–211.

Hyndman, R. D. & Klemperer, S. L., 1989. Lower-crustal porosity from electrical measurements and inferences about composition from seismic velocities, *Geophys. Res. Lett.,* **16,** 255–258.

Hyndman, R. D. & Shearer, P. M., 1989. Water in the Lower continental crust: Modelling magnetotelluric and seismic results, *Geophys. J. Int.,* **98,** 343–365.

Jones, A. G., 1992. Electrical conductivity of the continental lower crust, in: *Continental Lower Crust,* eds Fountain, D. M., Shaw, R. & Kay, R. W., Elsevier, Amsterdam.

Kellett, R. L., Mareschal, M. & Kurtz, R. D., 1992. A model of lower crustal electrical anisotropy for the Pontiac Subprovince of the Canadian Shield, *Geophys. J. Int.,* **111,** 141–150.

Kurtz, R. D., Niblett, E. R., Craven, J. A., Stevens, R. A. & Macnae, J. C., 1988. Electromagnetic studies over the Kapuskasing structural zone, in *Proceedings of the Kapuskasing Lithoprobe Workshop, Toronto, 16–17 Feb. 1988,* pp. 169–175, eds West, G. F.

Mjelde, R., 1992. Shear waves from 3-C ocean bottom seismographs off Lofoten, Norway, indicative of anisotropy in the lower crust, *Geophys. J. Int.,* **110,** 283–296.

Mjelde, R. & Sellevoll, M. A., 1993. Possible shallow crustal *S*-wave anisotropy off Lofoten, Norway, inferred from 3-C Ocean Bottom Seismographs, *Geophys. J. Int.,* **115,** 159–167.

Mjelde, R., Sellevoll, M. A., Shimamura, H., Iwasaki, T. & Kanazawa, T., 1992. A crustal study off Lofoten, N. Norway, by use of 3-component ocean bottom seismographs, *Tectonophysics,* **212,** 269–288.

Mjelde, R., Sellevoll, M. A., Shimamura, H., Iwasaki, T. & Kanazawa, T., 1993. Crustal structure under Lofoten, N. Norway, from vertical incidence and wide-angle seismic data, *Geophys. J. Int.,* **114,** 116–126.

Mokhtari, M., 1991. A geological model for the Lofoten continental margin, *Dr. Scient. Thesis,* IFJ, University of Bergen.

Mokhtari, M., Pegrum, R. M. & Sellevoll, M. A., 1989. A geophysical study of the Norwegian continental margin between 67°N and 69°N, *SEISMO-SERIES,* **28,** IFJ, University of Bergen.

Mutter, J. C., 1984. Cenozoic and late mesozoic stratigraphy and subsidence history of the Norwegian Margin, *Bull. geol. Soc. Am.,* **95,** 1135–1149.

Neidell, N. S., 1985. Land application of *S* waves, *Geophys: Lead. Edge Explor.,* 32–44.

Rasmussen, T. M., 1988. Magnetotellurics in southwestern Sweden: evidence for electrical anisotropy in the lower crust? *J. geophys. Res.,* **93,** 7897–7907.

Richardson, S. W., Gilbert, M. C. & Bell, P. M., 1969. Experimental determination of kyanite–andalusite and andalusite–sillimanite equilibrium; the aluminium silicate triple point, *Am. J. Sci.,* **267,** 259–272.

Rønnevik, H. C., Eggen, S. & Vollset, J., 1983. Exploration of the Norwegian Shelf, in *Petroleum Geochemistry and Exploration of Europe,* pp. 71–94, eds Brooks, J., Blackwell, Oxford.

Rutter, E. H. & Brodie, K. H., 1992. Rheology of the lower crust, in *Continental Lower Crust,* pp. 201–269, eds Fountain, D. M., Arculus, R. & Kay, R. W., Elsevier.

Sellevoll, M. A., 1973. Mohorovicic discontinuity beneath Fennoscandia and adjacent parts of the Norwegian Sea and North Sea, *Tectonophysics,* **20,** 359–366.

Sellevoll, M. A., 1988. Seismiske undersøkelser av Lofoten Marginen og refleksjonsseismiske test-målinger på Mohns Rygg, M/S Håkon Mosby, 29 juli–19 august 1988, *Cruise report,* IFJF. University of Bergen.

Sellevoll, M. A. & Thanvarachorn, P., 1977. A seismic reconnaissance study of the earth's crust in the Lofoten–Vesterålen area, northern Norway, in *The Norwegian Geotraverse Project,* pp. 101–113, Heier, K. S., Norg. Geol. Unders., Trondheim.

Shimamura, H., 1988. OBS technical description, *Annexe to Cruise Report by Sellevoll.*

Skogseid, J. & Eldholm, O., 1989. Vøring plateau continental margin: Seismic interpretation, stratigraphy and vertical movements, in *Proc. ODP, Sci. Results, 104,* pp. 993–1030, eds Eldholm, O., Thiede, J. & Taylor, E., Ocean Drilling Program, College Station, TX.

Soper, N. J., Strachan, R. A., Holdsworth, R. E., Gayer, R. A. & Greiling, R. O., 1992. Sinistral transpression and the Silurian closure of Iapetus, *J. geol. Soc. Lond.,* **149,** 871–881.